Available online at www.sciencedirect.com
SCIENCE DIRECT®
Ecological Modelling 187 (2005) 281–296
ECOLOGICAL MODELLING
www.elsevier.com/locate/ecolmodel

Estimating estuarine gross production, community respiration and net ecosystem production: a nonlinear inverse technique

J.J. Vallino *, C.S. Hopkinson, R.H. Garritt

Ecosystems Center, Marine Biological Laboratory, 7 MBL St., Woods Hole, MA 02050, USA

Received 21 July 2003; received in revised form 12 October 2004; accepted 21 October 2004
Available online 23 February 2005

Abstract

We describe a nonlinear inverse technique to estimate gross primary production (GPP), community respiration (CR), and net ecosystem production in the vertically well mixed Parker River, Plum Island Sound estuarine system located in northeastern Massachusetts, USA. The approach uses a calibrated 1D advection–dispersion model to predict oxygen and salt concentrations along the estuarine length, which are compared to oxygen concentrations measured during high speed transects near dawn and dusk over a 2-day period in June 1995. The spatiotemporal shapes of the GPP and CR surfaces are represented with cubic B-splines that are deformed as needed by an algorithm that seeks to minimize error between oxygen observations and model predictions. The spatially resolving solution shows maximum instantaneous GPP of 1030 mmol O_2 m^{-3} d^{-1} and CR of 340 mmol O_2 m^{-3} d^{-1} in the upper portions of the estuary; however, the overall estuary is net heterotrophic (-4.8 Mg C d^{-1}). Analysis of the advection–dispersion model reveals that gas invasion and longitudinal dispersion account for up to 21 and 14% of local O_2 accumulation relative to CR, respectively. However, an oxygen balance averaged over the 2-day sampling period shows that the negative net ecosystem productivity is balanced by a loss in estuarine oxygen storage. Carbon budget analysis indicates that terrestrial, marine, and marsh allochthonous inputs account for 2, 27 and 71% of the observed net heterotrophy, respectively.

Keywords: Inverse modeling; Estuarine metabolism; Gross primary production; Community respiration; Dissolved oxygen; LTER

1. Introduction

Diurnal changes in oxygen concentration have long been used to estimate gross primary production (GPP), community respiration (CR, taken as a positive number here) and net ecosystem productivity (NEP) in aquatic systems (Odum, 1956). Although stoichiometrically constrained mass balance models are also used to estimate system metabolism (Smith and Hollibaugh, 1997; Kemp et al., 1997; Perez et al., 2000), the dissolved oxygen (DO) method requires fewer assumptions and measurements. Both approaches are types of inverse modeling, in which measurements (DO) are combined with mass balance models to estimate processes not directly measured (GPP, CR, and NEP). There are also dynamic, or state space, models that use dissolved oxy-

* Corresponding author. Tel.: +1 508 289 7648; fax: +1 508 457 1548.
E-mail address: jvallino@mbl.edu (J.J. Vallino).

0304-3800/$ – see front matter © 2005 Elsevier B.V. All rights reserved.
doi:10.1016/j.ecolmodel.2004.10.018

gen measurements to calibrate prognostic water quality models that estimate GPP, CR, and NEP (e.g., Park et al., 1996). However, these models require extensive measurements of other variables to calibrate model parameters, and predicted processes can diverge significantly from their true values unless data assimilation techniques are used (Vallino, 2000). In this manuscript we only consider the inverse modeling approach.

Most DO inverse methods are based on the following observation. During daylight hours, oxygen concentration increases due to net daytime production (NDP) and decreases during the night time due to CR. By assuming that CR is unaffected by light, gross daytime production (GDP) can be estimated by adding CR, measured in the dark, to NDP, and GPP and NEP can be obtained by integrating GDP and NDP – CR over a 24 h period, respectively. Two basic methodologies have been developed for measuring GPP, CR, and NEP: bottle/chamber methods (Gaarder and Gran, 1927; Odum and Hoskin, 1958) or in situ, whole (or open) system methods (Odum, 1956). In the former method, water samples are placed in a bottle (or a chamber over sediments) and some of the samples are exposed to ambient light to get net daytime production (NDP), while others are kept in the dark to get CR. In whole system methods, in situ oxygen probes are used to measure diurnal changes in the oxygen at either a single location (Welch, 1968), or, in flowing systems, at upstream and downstream locations (Odum, 1956). The DO methods have been widely applied in streams (Gulliver and Stefan, 1984c; Marzolf et al., 1994; Young and Huryn, 1999; Mulholland et al., 2001), lakes (Welch, 1968; Cole et al., 2000) and estuaries (Hopkinson, 1985; Caffrey et al., 1998; Perez et al., 2000). While both methods have their pros and cons (Swaney et al., 1999; Young and Huryn, 1999), the whole system method is preferred in most situations, as the whole system is typically the study of interest. The requirement to estimate oxygen gas transfer across the air–water interface, and to properly account for advective and dispersive transport of oxygen in lotic systems means that computational models are often required to obtain accurate estimates for GPP, CR, and NEP.

Since Odum's (1956) original work, several refinements have been made to the whole system method (Marzolf et al., 1994; Young and Huryn, 1998), including means to estimate the gas transfer coefficient directly (Gulliver and Stefan, 1984b; Leclercq et al., 1999) or through the addition of tracers (Genereux and Hemond, 1992), as well as relaxing the assumption of light independent respiration (Parkhill and Gulliver, 1999). To better account for temporal variations in NEP, Kelly et al. (1974) approximated NEP with a truncated Fourier cosine series, which they demonstrated improved NEP numerical precision. Exact solution to the stream advection equation also improves NEP estimation (Hornberger and Kelly, 1972). Portielje et al. (1996) computational model accounts for light intensity and temperature effects, and employed a two box model to account for vertical stratification. The Gulliver and Stefan (1984a) dissolved oxygen routing model (DORM) is perhaps the most comprehensive computation model for estimating GPP and CR in streams. DORM employs a 1D advection–dispersion model to account for spatial variability in DO concentration, gas exchange, and river morphology and also accounts for longitudinal dispersion. However, DORM operates under the two-station methodology (upstream–downstream), so does not provide spatial information on GPP and R, and cannot be applied in estuarine environments.

Because it is necessary to measure DO changes in the same water mass, estuarine and coastal environments present a challenge for the diel DO method due to the complexity of tracking water masses in tidal and ocean currents (Kemp and Boynton, 1980). Consequently, most GPP and CR estimates in estuaries are based on light-dark bottle incubations, or bottle incubations combined with a GPP model (Caffrey et al., 1998), so that water masses need not be followed. However, Swaney et al. (1999) developed a statistically based model to estimate GPP and CR from DO measurements by using salinity as a tracer of estuarine water parcels. Although their model accommodates vertical gradients in DO profiles, it spatially aggregates the data, so information on spatial distributions of GPP and CR are lost, and their use of a linear regression model degrades accuracy.

In this manuscript, we combine a 1D advection–dispersion model with a nonlinear inverse technique to estimate GPP, CR and NEP from near-synoptic measurements of DO in the Plum Island Estuary (PIE), MA. The primary advantage of our approach compared to those discussed above is that it can be applied in systems with time varying transport characteristics, typically found in estuaries,

and provides high-resolution spatiotemporal estimates of GPP, CR and NEP. The methodology is general, so is applicable to other vertically well-mixed systems.

2. Site description

The study was conducted in the Plum Island Sound Estuary in northeastern Massachusetts, USA (Fig. 1). The estuary and its watersheds lie within the Seaboard Lowland section of the New England physiographic province (Fenneman, 1938). The rivers and estuary discharge into the Gulf of Maine, a semi-enclosed sea off the Atlantic Ocean. The Gulf of Maine coastal current flows to the south along the coast. Coastal salinity varies seasonally in relation to land runoff and has a major influence on Plum Island Sound salinity (Blumberg et al., 1993).

The Plum Island Sound Estuary is a coastal plain, bar-built estuary with extensive areas of productive, tidal marshes. Tides are semi-diurnal with an average tidal range of 2.9 m and a spring-neap range of 2.6–4.0 m. Marshes typically flood only during spring tides. Estimated tidal prism is about 48×10^6 m^3. Mean depth increases along the length of the estuary from about 1.4 m at the head of the estuary to about 5.7 m, 11 km downstream at the head of the sound. Depths then decrease through the broad shallow sound to about 1.8 m prior to increasing to about 4.7 m at the mouth of the estuary. The large tides combined with the shallow depths and low freshwater inputs results in a vertically well mixed estuary with type 1A circulation (Hansen and Rattray, 1966). Water body area ranges from 12.8 to 20.0 km^2 from low to high tide. There are extensive areas of nonvegetated, intertidal flats at low tide (7.2 km^2). In this estuary where the typical spacing of topographic features is considerably less than the tidal

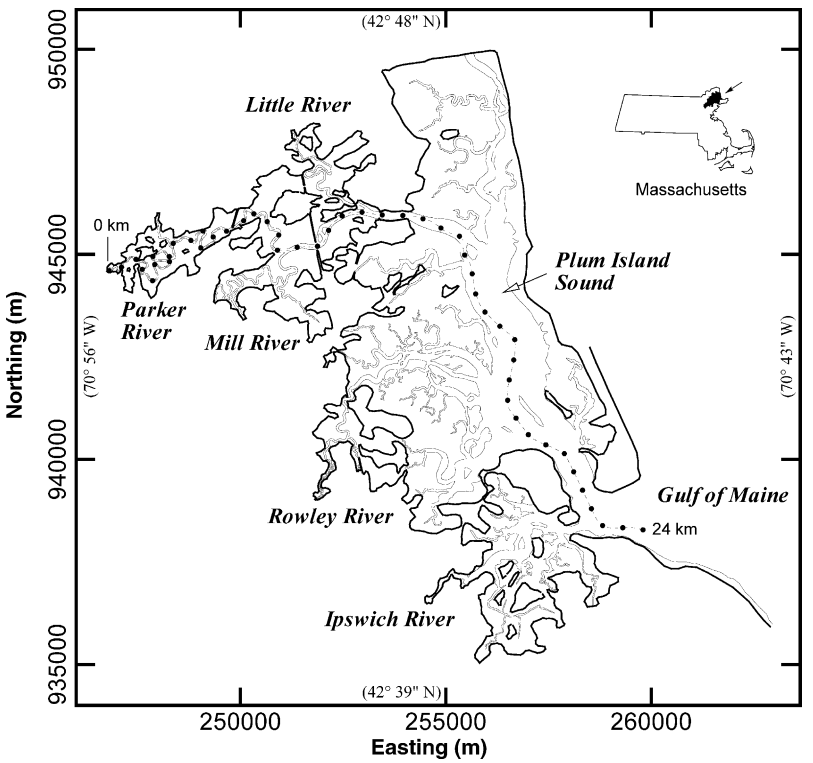

Fig. 1. Map of Plum Island Estuary located in northeastern Massachusetts, USA. Estuary marsh delimited by uplands (bold lines) and riverbanks (thin lines). Dotted line represents longitudinal axis of model ticked at half km intervals beginning at head of Parker River. Coordinates are Massachusetts Mainland State Plane 2001 (m) including geographic coordinates (NAD 83) of map boundaries in parentheses.

excursion and tidal amplitude is of the same order as average depth, tidal shear dispersion is probably the primary mechanism contributing to mixing (Smith, 1977; Geyer and Signell, 1992). Annual water temperature range is from −1.0 to 28 °C and salinity range is from 0 to 32. Vegetation is typical of New England marshes, the major wetland species being *Spartina alterniflora* and *S. patens* in brackish and saline regions and *Typha*, *Scirpus* and *Carex* in fresh water regions. Of the total estuarine area of 59.8, 39.8 km^2 is occupied by fresh- or saltwater marsh.

The 608.9 km^2 watershed draining into the estuary has two major rivers, the Parker and Ipswich Rivers, and eight secondary creeks. The USGS monitors discharge for 55.2 and 323.8 km^2 portions of the Parker and Ipswich Rivers, respectively. Discharge from ungauged portions of the watershed is estimated from area:discharge relations calculated for the gauged portion of the Parker River (Vallino and Hopkinson, 1998). Average annual discharge for the Parker River is 1.0 $m^3\,s^{-1}$, ranging seasonally from 0.2 $m^3\,s^{-1}$ in summer to 2.4 $m^3\,s^{-1}$ in winter. Calculated average annual discharge for the entire watershed draining into the estuary is 11.0 $m^3\,s^{-1}$. Discharge is thus about 67 times lower in volume than a single tidal prism. Precipitation is evenly distributed throughout the year and averages 112 cm y^{-1}, 44% of which is returned to the atmosphere via evapotranspiration (Sammel, 1967). Air temperature fluctuates annually between an average winter minimum of −7 °C and an average summer maximum of about 28 °C.

Based largely on estuarine metabolic patterns and tidal excursion lengths, we have identified four regions of interest in the estuary: upper (0–5.2 km, high tide volume 0.58 Mm^3), mid (5.2–9.3 km, 1.5 Mm^3), and lower (9.3–14.3 km, 4.8 Mm^3) portions of the Parker River and the sound (14.3–24 km, 33 Mm^3 – Fig. 1). Average tidal excursion at the mid-point of these regions is approximately 4, 6, 14, and greater than 14 km, respectively.

3. Field methods

Dissolved oxygen, salinity, and temperature were measured with a Hydrolab water quality sonde (Hydrolab Corp.) that was calibrated for DO in air at sea level just prior to sampling. Salinity was calibrated with KCl standards at concentrations of 0.5, 0.01, and 0.001 M, which have specific conductances (25 °C) of 58.64, 1.413, and 0.147 mS cm^{-1}, respectively. Oxygen, salinity, and temperature transects were taken between dawn and dusk along the Parker River and Plum Island Sound centerline starting at the estuarine mouth (24 km) and ending at the Parker River dam (0 km) (Fig. 1) on eight occasions between 27 and 29 June 1995. To obtain near-synoptic observations for each transect, the Hydrolab sonde was connected to a 500 ml flow through cell that was fed by a 18 mm ram tube mounted on the boat transom, which provided surface water samples while the boat was underway (Madden and Day, 1992). At a boat speed of 13 km h^{-1}, transects along the length of the estuary took approximately 1 h to complete, and data and location were recorded every 2 min.

4. Model description

To account for transport (and reaction) of salt and oxygen, the one-dimensional advection–dispersion, tidally averaged model of the form:

$$A(\bar{x})\frac{\partial \mathbf{c}(\bar{x},t)}{\partial t} = \frac{\partial}{\partial \bar{x}}\left(D(\bar{x})A(\bar{x})\frac{\partial \mathbf{c}(\bar{x},t)}{\partial \bar{x}} - q(\bar{x},t)\mathbf{c}(\bar{x},t)\right) + \sum_{i=1}^{\ell}\left(\mathbf{c}_{li}(t)\frac{\partial q_i(\bar{x},t)}{\partial \bar{x}}\right) + A(\bar{x})\phi(\bar{x},t) \quad (1)$$

developed and calibrated for the Parker River–Plum Island Sound system (Vallino and Hopkinson, 1998) was used, where the vector $\mathbf{c}(\bar{x},t)$ is concentration of salt and oxygen, $[c_s, c_{O_2}]^T$ (mmol m^{-3}), $A(\bar{x})$ is the river cross-sectional area (m^2) at high tide, $D(\bar{x})$ the longitudinal dispersion ($m^2\,d^{-1}$), $q(\bar{x},t)$ the cumulative freshwater discharge ($m^3\,d^{-1}$), $\mathbf{c}_{li}(t)$ the salt and oxygen concentration in lateral input i, the vector $\boldsymbol{\phi}(\bar{x},t)$ is the production rate of salt and oxygen (mmol $m^{-3}\,d^{-1}$), and $\bar{x}$ the location at high tide (m). Salinity transects and dye release studies were previously used to determine the dispersion coefficient in the Plum Island Estuary (Vallino and Hopkinson, 1998). It was found that the mode of transport in the Parker River (0–15 km) is highly dependent on freshwater input, while that in Plum Island Sound is typically governed by dis-

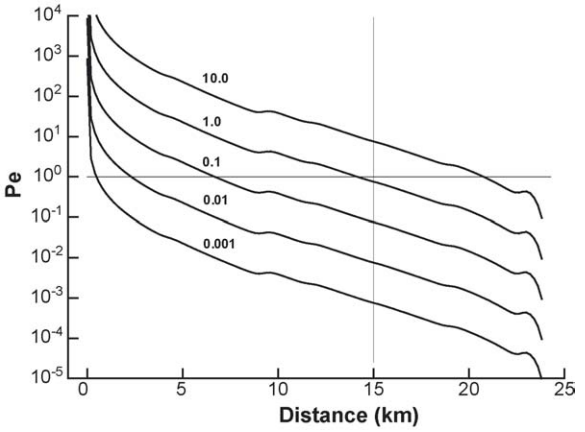

Fig. 2. Calculated Peclet Number (*Pe*) as a function of location along the main estuarine axis for different Parker River discharges ($m^3\ s^{-1}$). Parker River ends and Plum Island Sound begins at 15 km.

persive transport, as indicated by the Peclet number (Fig. 2), which is the ratio of advective to dispersive transport, $Pe = (q/A)/(D/L)$, where L is a characteristic length for dispersion (in this case 24 km). A Peclet number much greater than 1 indicates transport is advection dominated, while *Pe* much less than 1 indicates dispersion-dominated transport.

Boundary conditions (BC) on the freshwater side (or left side, *xL*) of the model domain are specified by a time dependent flux (i.e., Robin BC),

$$\left[D(\bar{x})A(\bar{x})\frac{\partial \mathbf{c}(\bar{x},t)}{\partial \bar{x}} - q(\bar{x},t)\mathbf{c}(\bar{x},t)\right]_{\bar{x}=xL} = -q_{xL}(t)\mathbf{c}_{xL}(t) \quad (2)$$

while Dirichlet boundary conditions are employed for the marine end member (or right side, *xR*),

$$\mathbf{c}(\bar{x},t)|_{\bar{x}=xR} = \mathbf{c}_{xR}(t) \quad (3)$$

where $q_{xL}(t)$, $\mathbf{c}_{xL}(t)$, and $\mathbf{c}_{xR}(t)$ are the freshwater discharge and concentrations of salt and oxygen in the freshwater and marine end member at time t, respectively. For the left boundary, it is assumed that oxygen is at saturation levels for the observed temperature of the freshwater. The USGS gaging station at Byfield, MA (Station 01101000) provided the daily freshwater discharge, which was weighted by relative watershed areas to obtain freshwater discharge at all seven inputs (Vallino and Hopkinson, 1998). Discharge averaged $0.06\ m^3\ s^{-1}$ during the study period. We used salinity and oxygen observations obtained from transects to set the right boundary conditions; linear interpolation was employed between observation times.

Observations from the first transect (27 June 1995, 20:00) were used to set the initial conditions for Eq. (1). However, since Eq. (1) is tidally averaged, predictions at any time correspond to locations at the virtual high tide, $\bar{x}$. Consequently, it was necessary to run a salt-only simulation to determine salinity locations corresponding to virtual high tide on 27 June 1995, 20:00, and then map the observations from transect 1 to these locations. By beginning the salt-only simulation a month prior to 27 June, initial salt concentrations did not need to be known, as the influence of initial conditions decay rapidly. Although it would have been possible to run salinity-oxygen simulations a month prior to observations so that initial conditions would not need to be known, this would have significantly increased computation time in the optimization phase discussed below.

The only unknown in Eq. (1) is the oxygen production rate, ϕ_{O_2}. Oxygen production is affected by water column and benthic gross production and community respiration and by exchange across the air–water interface as given by,

$$\phi_{O_2}(\bar{x},t) = P(\bar{x},t) - R(\bar{x}) + \frac{k_{O_2}}{h(\bar{x})}(c^*_{O_2}(c_S,T) - c_{O_2}(\bar{x},t)) \quad (4)$$

where $P(\bar{x},t)$ is the gross primary productivity (GPP) ($mmol\ m^{-3}\ d^{-1}$), $R(\bar{x})$ the community respiration (CR) ($mmol\ m^{-3}\ d^{-1}$), k_{O_2} the oxygen gas transfer velocity ($m\ d^{-1}$), $h(\bar{x})$ the high tide water column depth (m) obtained from field surveys, and $c^*_{O_2}(c_S,T)$ the oxygen saturation concentration at salinity c_S and temperature T, as given by Weiss (1970). Sulfur hexafluoride (SF_6) tracers studies used to estimate k_{O_2} in the Parker River found values range from 0.5 to $1.5\ m\ d^{-1}$ (Carini et al., 1996). Since predicting k_{O_2} in estuaries is problematic due to complex hydrodynamics (Jahne et al., 1987), we choose to keep k_{O_2} fixed at $1.0\ m\ d^{-1}$ for this study.

The primary objective of this study was to develop a means to determine the remaining unknowns in Eq. (4), $P(\bar{x},t)$ and $R(\bar{x})$. The basic methodology to estimate $P(\bar{x},t)$ and $R(\bar{x})$ is to set-up an optimization problem in which an initial guess is provided for $P(\bar{x},t)$ and $R(\bar{x})$, which then allows the integration of Eq. (1). Dissolved

oxygen concentration estimates from Eq. (1) can then be compared to transect data to generate a residual error that can be used to improve $P(\bar{x}, t)$ and $R(\bar{x})$ estimates, which are then used in Eq. (1) to generate better DO estimates. This iteration proceeds until a local minimum is obtained.

In estuaries, $P(\bar{x}, t)$ and $R(\bar{x})$ can have strong spatial gradients and $P(\bar{x}, t)$ changes over time because of changes in light intensity, so we chose to express $P(\bar{x}, t)$ and $R(\bar{x})$ as functions of location and time, and location only, respectively. However, because transects were not run at high tide, DO at virtual high tide locations, $\bar{x}$, predicted by Eq. (1) at time t do not correspond to actual observed locations, x, at time t. To overcome this problem, model predictions and observations were compared in salinity space, which is tide independent. At any time, a function exists to map between salinity, c_S, and $\bar{x}$, and because c_S is always a monotonically increasing function of $\bar{x}$ (and x) in the PIE system, the inverse function exists as well, so that:

$$c_S = \zeta(\bar{x}) \quad \text{and} \quad \bar{x} = \zeta^{-1}(c_S) \tag{5}$$

To represent $P(\bar{x}, t)$ and $R(\bar{x})$, we use the following cubic B-splines,

$$\left\{\{c_{S_i}, \hat{P}_i^M\}, \quad i = 1, n\right\} \xrightarrow{B_n^3} \pi_n(c_S) \tag{6}$$

$$\left\{\{c_{S_i}, \hat{R}_i\}, \; i = 1, n\right\} \xrightarrow{B_n^3} \rho_n(c_S) \tag{7}$$

where the nomenclature indicates that the interpolating functions $\pi_n(c_S)$ and $\rho_n(c_S)$ are constructed from two sets of n points using cubic B-splines, and $\hat{P}_i^M$ and $\hat{R}_i$ are estimates of maximum GPP and CR at salinity c_{S_i}, respectively. This approach allows a smooth function over all salinity space to be generated from a small set of discrete points. By manipulating $\hat{P}_i^M$ and $\hat{R}_i$, arbitrary functions for $P(\bar{x}, t)$ and $R(\bar{x})$ can be readily generated by,

$$P(\bar{x}, t) = \frac{I(t)}{I^M}\pi_n\left(\zeta(\bar{x})\right) \quad \text{or} \quad P(c_S, t) = \frac{I(t)}{I^M}\pi_n(c_S) \tag{8}$$

$$R(\bar{x}) = \rho_n(\zeta(\bar{x})) \quad \text{or} \quad R(c_S) = \rho_n(c_S) \tag{9}$$

where $I(t)$ is photosynthetically active radiation (PAR) and I^M is the maximum value of $I(t)$ used for normalization. Because the transects were conducted on cloudless days, $I(t)$ was modeled (Brock, 1981; Baker and Frouin, 1987).

The optimization to obtain estimates for $P(\bar{x}, t)$ and $R(\bar{x})$ is as follows. The number of spline points, n, and values of c_{S_i} are specified, and initial guesses for $\hat{P}_i^M$ and $\hat{R}_i$ are provided. Using Eqs. (2)–(9), Eq. (1) is integrated over time and space to provide an estimate for oxygen concentration, $\hat{c}_{O_2}(\bar{x}, t_k)$, corresponding to times, t_k, when transect data are available. An iteration involving $\hat{P}_i^M$ and $\hat{R}_i$ commences to solve the optimization problem,

$$\underset{\hat{P}_i^M, \hat{R}_i}{\text{minimize}} \quad J = \sum_j \sum_k \left(\hat{c}_{O_2}(\zeta^{-1}(c_{S_j}), t_k) - \tilde{c}_{O_2}(c_{S_j}, t_k)\right)^2 \tag{10}$$

where $\tilde{c}_{O_2}(c_{S_j}, t_k)$ is the observed oxygen concentration at salinity c_{S_j} and time t_k. Linear interpolation was used to construct the inverse function, $\zeta^{-1}(c_S)$.

5. Numerical methods

We solved the 1D PDE, Eq. (1), using the moving grid routine of Blom and Zegeling (1994) on a 100-node grid. The conjugate-gradient-based routine PRAXIS (Brent, 1973), which does not require gradient information on the function, was used to find the minimum of Eq. (10). Since PRAXIS does not permit constraints on the parameter search space, simple box constraints of the form

$$\hat{R}_i\big|_{\min} \le \hat{R}_i \le \hat{R}_i\big|_{\max} \quad \text{and}$$
$$\hat{P}_i^M\big|_{\min} \le \hat{P}_i^M \le \hat{P}_i^M\big|_{\max} \tag{11}$$

were implemented by transforming the parameter space by a sine-squared transform (Box, 1966; Vallino, 2000), where all minimum bounds were set to 0, and all maximum bounds to 1500 mmol m^{-3} d^{-1}. The PRAXIS parameter values that produced the best performance were tolerance (T0) at 10^{-4}, maximum step size (H0) at 0.2 and ill-conditioned problem (ILLC) set to false. Initial guesses for $\hat{P}_i^M$ and $\hat{R}_i$ ranged from 100 to 500 mmol m^{-3} d^{-1}. The routines DBINT4 and DBVALU from the SLATEC library (Vandevender and Haskell, 1982) were used to construct and interpolate

the cubic B-splines, respectively. The cubic B-splines were fit through 12 points at salinities 0, 1, 2, 3, 5, 7, 9, 12, 15, 22, 27, 31 for both $\pi_n(c_S)$ and $\rho_n(c_S)$. Numerical quadrature of GPP, CR, and NEP surfaces was conducted by first interpolating surfaces onto regular grids using routines TRMESH (Renka, 1996b) and INTRC0 (Renka, 1996a) and then employing routine ADAPT of the National Institute of Standards and Technology (NIST) Core Math Library (CMLIB) for integration. All the above Fortran routines are in the public domain and can be obtained at Netlib Repository (Dongarra and Grosse, 1987), except for CMLIB, which is available from NIST (ftp://ftp.nist.gov/pub/cmlib/). Double precession (8 byte) was used for all Fortran computations.

6. Model error analysis

Although sources of error include those associated with transect measurements (oxygen, salinity, temperature and discharge), model parameterization (dispersion and gas exchange coefficients), and model approximation of true physics, the largest sources of variability in estimating GPP and CR reside with solution of the optimization problem, Eq. (10). In nonlinear problems, the hyper-surface defined by Eq. (10) often contains many local optima (Vallino, 2000). Although it is desirable to locate the global optimum, except for special cases, it is not possible to determine if a particular optimum is the global optimum. Furthermore, from a practical perspective, the global optimum solution may not possess properties that make it superior than other local optima of similar cost. For well-posed problems, different local optima should provide similar values for the parameters being sought; however, poorly posed or underdetermined problems may produce vastly different parameter values at local optima of similar magnitude. To examine the impact of different local optima of Eq. (10) on estimating $P(\bar{x}, t)$, Eq. (8), and $R(\bar{x})$, Eq. (9), we examined the solutions to Eq. (10) at nine other optima whose cost, J, were less than 20% greater than the minimum value of J found. Local optima were obtained by changing the initial guess for $\hat{P}_i^M$ and $\hat{R}_i$ as well as the parameter values associated with the optimization routine PRAXIS.

7. Results

The diel variation in oxygen, exceeding 100 mmol m^{-3}, is clearly evident between the dawn and dusk transects conducted between 27 and 29 June 1995 (Fig. 3). Transects conducted between 15:00 and 20:15 (dusk) exhibit elevated DO, while those conducted between 6:30 and 11:00 of the next day show depressed DO. Dissolved oxygen only exhibited super saturation near the head (salinity < 4 practical salinity unit (PSU)) and mouth (salinity > 30 PSU) of the estuary. At all other salinities, DO was either at or below saturation, which indicates that respiration generally exceeded primary production (i.e., heterotrophic) on the observed days. There was also a reproducible sag in DO mid-estuary, from approximately 14 to 28 PSU, which was always under saturated.

To examine solution variability, the minimization problem (J, Eq. (10)) was solved 30 times, with each run conducted from a different initial guess. Although each run produced a unique local minimum, the 10 best solutions had final costs ranging from 12,400 to 14,660 (mmol m^{-3})^2. PRAXIS required between 1000 and 9000 integrations of Eq. (1) to locate a minimum, which utilized between 1.3 and 11.5 min of CPU time on an AMD Athlon XP 3000+ processor operating at 2.16 GHz. For the best 10 local

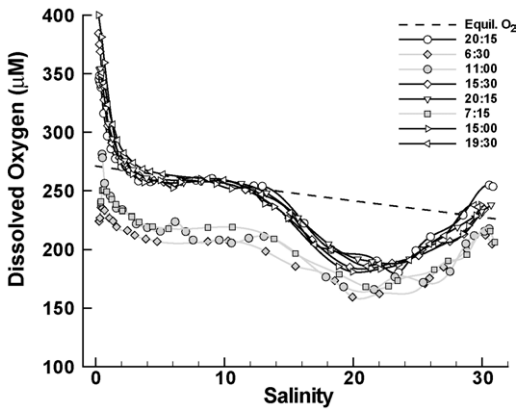

Fig. 3. Dissolved oxygen (DO) concentrations as a function of salinity measured along the estuarine axis. Transects were conducted on the 27th, 28th and 29th of June 1995 at the indicated times and are categorized as either "dawn" (gray lines and symbols) or "dusk" (black lines, open symbols) runs. Dotted line shows DO concentration at equilibrium with air corrected for salinity and temperature.

optima, the predicted DO transects match the observed DO transects well (Fig. 4); however, all optima produced DO curves that slightly over estimate observed DO at 11:00 28 June 1995 (Fig. 4(C)) while slightly under estimating DO at 7:15 29 June 1995 (Fig. 4(F)). Although 10 different local minimums of Eq. (10) were found, all solutions were similar, as shown by the standard deviations of $\hat{P}_i^{\mathrm{M}}$ and $\hat{R}_i$ at each spline knot (Fig. 5). Consequently, we will focus analysis on the best solution ($J = 12{,}400$) with-

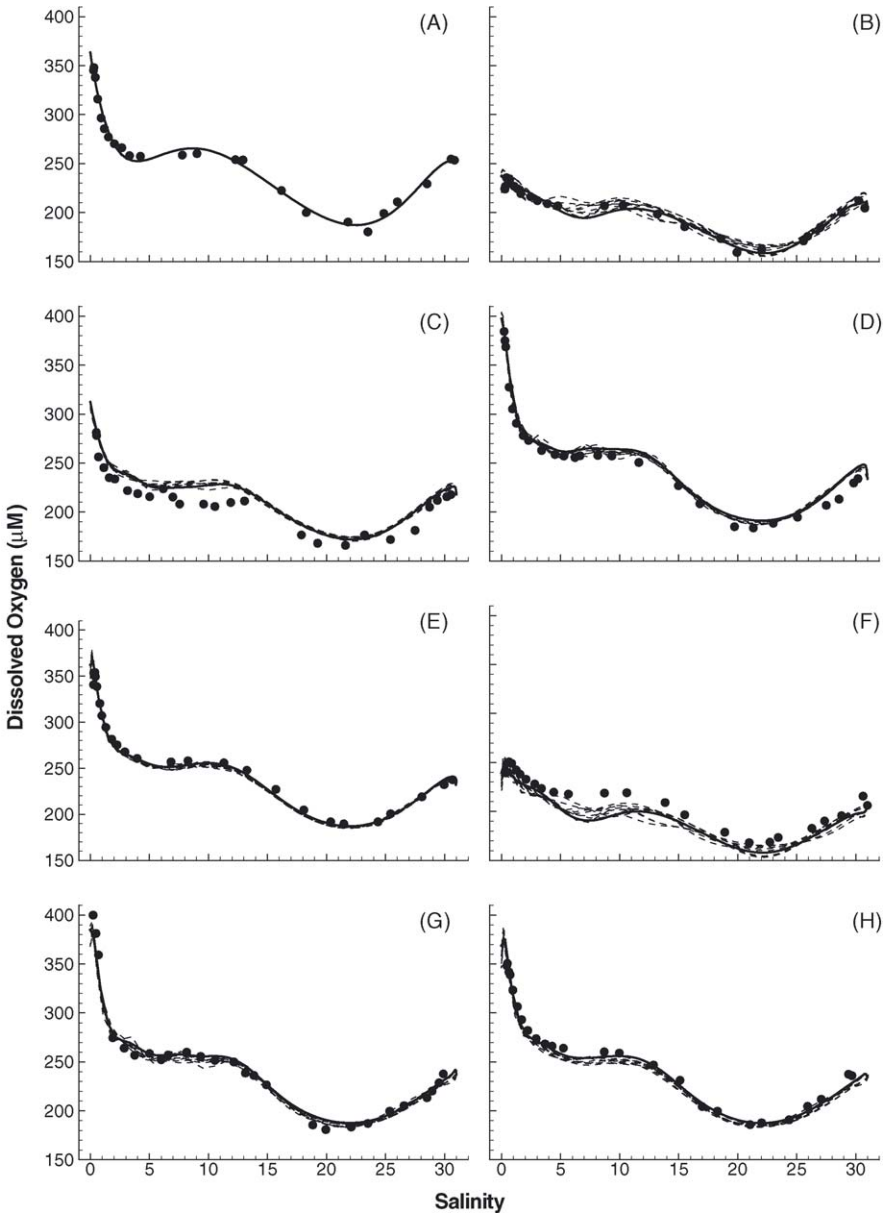

Fig. 4. Comparison of all 10 simulated (lines) to observed (symbols) dissolved oxygen concentration following data assimilation as a function of salinity along estuarine transect at times (A) 20:15 27 June 1995, (B) 6:30, (C) 11:00, (D) 15:30, (E) 20:15 28 June 1995, (F) 7:17, (G) 15:00, (H) 19:30 29 June 1995. Best local minimum solution is shown as solid line, while others are dashed.

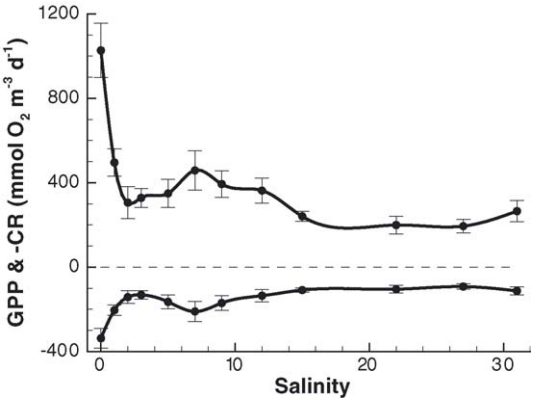

Fig. 5. Estimated instantaneous gross primary production (GPP, positive value) and community respiration (−CR, negative value) at 12:00 along the estuarine transect obtained from the best local minimum solution of the minimization problem, Eq. (10). Circle symbols correspond to location of spline knots, Eqs. (6) and (7), and error bars represent ±1 standard deviation from all 10 solutions.

out loss of generality. The production and respiration functions obtained from the minimization of J sampled at 12:00 h (Fig. 5) show very high productivity (>1000 mmol O_2 m^{-3} d^{-1}) and respiration in the upper estuary (0–2 PSU) and a much smaller secondary peak around 7 PSU. From approximately 16 PSU onward, GPP and CR are relatively constant, except for a sight increase at the estuarine mouth (Fig. 5). These productivities might appear unrealistically high compared to typically reported values; however, rates reported in the literature are average rates over a 24 h period, while that shown in Fig. 5 are maximum *instantaneous* rates. To examine daily-averaged rates, it is necessary to add the temporal axis and integrate over the surfaces.

Fig. 6 illustrates estimated GPP (Fig. 6(A)) and CR (Fig. 6(B)) at any time and location within the estuary during the period when transects were conducted (shown as lines parallel to salinity axis on surface plots). The temporal nature of GPP caused by time varying PAR, Eq. (8), is clearly evident. By subtracting CR from GPP, NEP as a function of salinity and time can be generated (Fig. 6(C)). Depending on location and time, NEP can be either positive or negative; however, in order to determine whether NEP is positive or negative over a 24 h period, the surface must be averaged over one day, Δt, as given by:

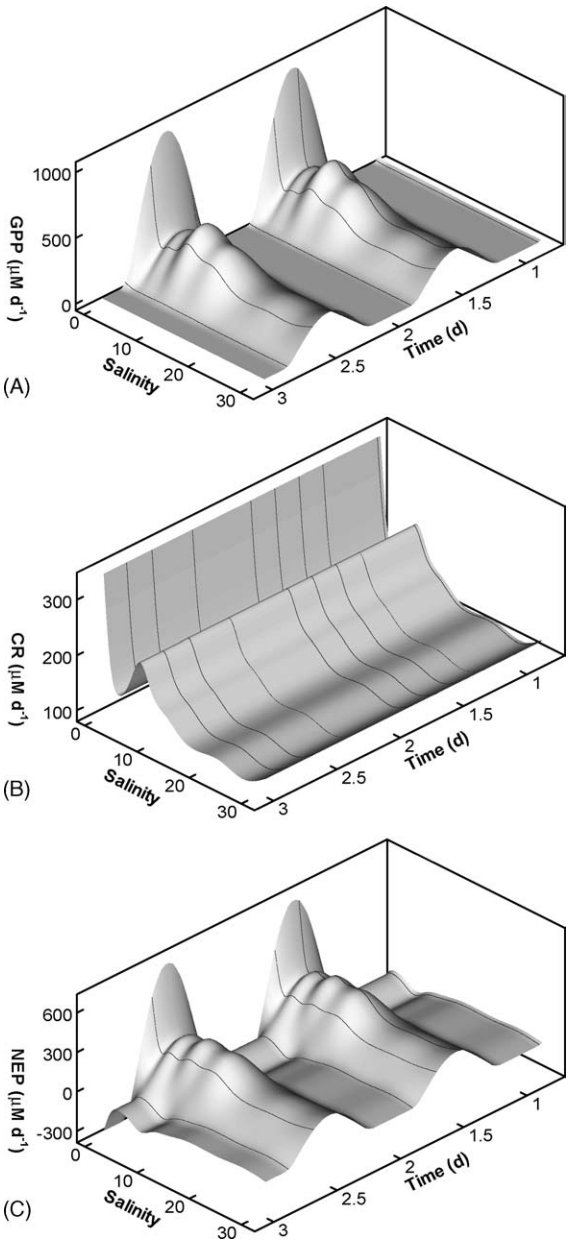

Fig. 6. Estimated instantaneous gross primary production (GPP), community respiration (CR) and net ecosystem productivity (NEP) as a function of salinity along estuarine transect and time obtained from best solution of minimization problem, Eq. (10). Thin black lines on surface indicate times when transects were conducted. Time 0 corresponds to 0:00 27 June 1995.

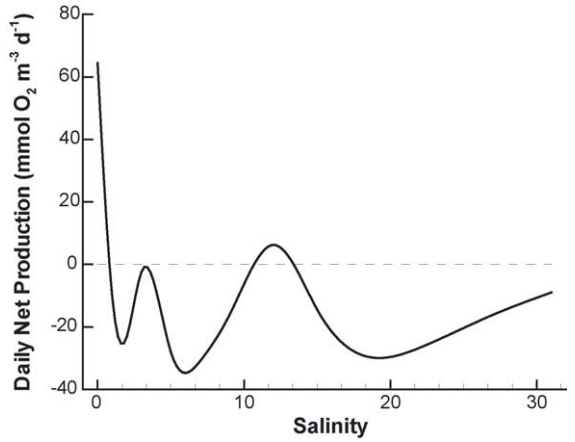

Fig. 7. Net ecosystem production per m^3 integrated over a 24 h period as a function of salinity along estuarine axis for $J = 12{,}400$ solution.

$$\langle N(c_S)\rangle_V = \frac{1}{\Delta t}\int_t^{t+\Delta t} P(c_S,t) - R(c_S)\,dt \quad \text{or}$$

$$\langle N(\bar{x})\rangle_V = \frac{1}{\Delta t}\int_t^{t+\Delta t} P(\bar{x},t) - R(\bar{x})\,dt \tag{12}$$

where $\langle N()\rangle_V$ is daily averaged NEP as a function of salinity, c_S, or, location at high tide, $\bar{x}$. Daily averaged NEP (Figs. 7 and 8) clearly shows that net autotrophy (NEP > 0) only occurs in the top 1 km of the estuary, or above 1 PSU, and slightly again around 4 km (or ca. 12 PSU). The remaining parts of the estuary are net heterotrophic (NEP < 0).

Depth integrated rates, $\langle\rangle_D$, converted to carbon equivalents ($g\,C\,m^{-2}\,d^{-1}$) are obtained by integrating as follows,

$$\langle P(c_S)\rangle_D = \frac{\omega_C}{1000\Delta t}\frac{1}{\theta_P}\int_t^{t+\Delta t} P(c_S,t)h(\zeta^{-1}(c_S))\,dt \tag{13}$$

$$\langle R(c_S)\rangle_D = \frac{\omega_C\theta_R}{1000\Delta t}\int_t^{t+\Delta t} R(c_S)h(\zeta^{-1}(c_S))\,dt = \frac{\omega_C\theta}{1000\Delta t}R(c_S)h(\zeta^{-1}(c_S)) \tag{14}$$

$$\langle N(c_S)\rangle_D = \langle P(c_S)\rangle_D - \langle R(c_S)\rangle_D \tag{15}$$

where ω_C is the molecular weight of C, θ_P the photosynthetic quotient (moles O_2 evolved/mol CO_2 consumed) and θ_R the respiratory quotient (mol CO_2 produced/mol O_2 consumed), both assumed equal to one here (Williams and Robertson, 1991; Laws, 1991; Robinson and Williams, 1999). Because depth does not vary greatly over the length of the estuary, depth integrated rates (Fig. 9) are spatially similar to the volumetric-based rates, and

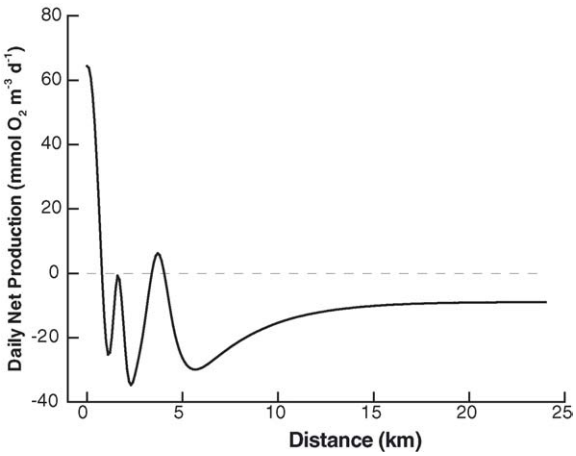

Fig. 8. Net ecosystem production per m^3 integrated over a 24 h period as a function of distance at high tide along estuarine axis for $J = 12{,}400$ solution.

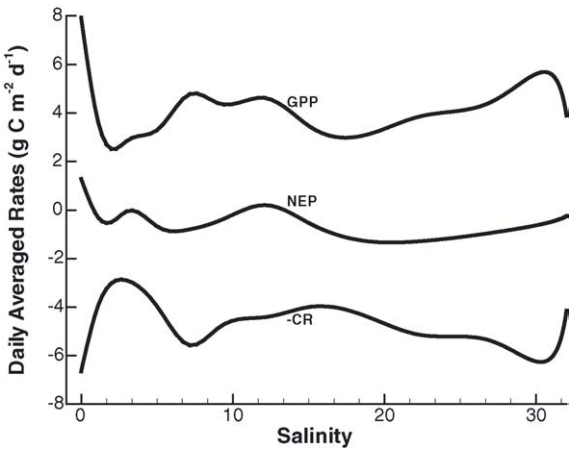

Fig. 9. Depth integrated gross primary production (GPP), community respiration (−CR, plotted as negative value) and net ecosystem production (NEP) integrated over a 24 h period as a function of salinity along estuarine axis for $J = 12{,}400$ solution.

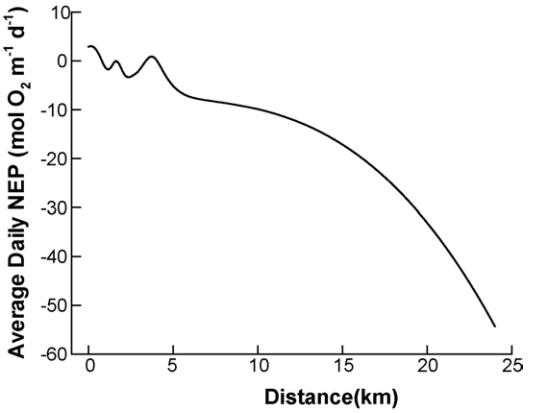

Fig. 10. Longitudinal net ecosystem production integrated over a 24 h period as a function of distance at high tide along estuarine axis for $J = 12{,}400$ solution.

the auto- and heterotrophic status of the estuary is unaltered.

Volumetric (Eq. (12)) and depth integrated (Eq. (15)) daily averaged NEP estimates give a biased perception to the overall trophic status of the estuary because they to not account for the fact that the cross-sectional area of the estuary greatly increases from the freshwater to the marine end-member. Longitudinally based daily averaged NEP (mol O_2 m^{-1} d^{-1}) is given by,

$$\langle N(\bar{x})\rangle_{\mathrm{L}} = \frac{1}{\Delta t}\int_{t}^{t+\Delta t} (P(\bar{x},t) - R(\bar{x}))A(\bar{x})\,\mathrm{d}t \qquad (16)$$

By accounting for estuarine cross-section, $\langle N(\bar{x})\rangle_{\mathrm{L}}$ shows the overall estuary is highly heterotrophic per meter (Fig. 10). Finally, cumulative average daily NEP between an up estuarine location, $\bar{x}_{\mathrm{U}}$, and down estuarine location, $\bar{x}_{\mathrm{D}}$, is given by,

$$\begin{aligned}
\langle P(\bar{x}_{\mathrm{U}}|\bar{x}_{\mathrm{D}})\rangle_{\Sigma} &= \frac{\omega_{\mathrm{C}}}{1000\Delta t}\frac{1}{\theta_{\mathrm{P}}}\int_{\bar{x}_{\mathrm{U}}}^{\bar{x}_{\mathrm{D}}}\int_{t}^{t+\Delta t} P(\bar{x},t)A(\bar{x})\,\mathrm{d}t\,\mathrm{d}\bar{x}\\
\langle R(\bar{x}_{\mathrm{U}}|\bar{x}_{\mathrm{D}})\rangle_{\Sigma} &= \frac{\omega_{\mathrm{C}}\theta_{\mathrm{R}}}{1000}\int_{\bar{x}_{\mathrm{U}}}^{\bar{x}_{\mathrm{D}}} R(\bar{x})A(\bar{x})\,\mathrm{d}\bar{x}\\
\langle N(\bar{x}_{\mathrm{U}}|\bar{x}_{\mathrm{D}})\rangle_{\Sigma} &= \langle P(\bar{x}_{\mathrm{U}}|\bar{x}_{\mathrm{D}})\rangle_{\Sigma} - \langle R(\bar{x}_{\mathrm{U}}|\bar{x}_{\mathrm{D}})\rangle_{\Sigma}
\end{aligned} \qquad (17)$$

Integration of this equation shows that even the top 5 km of the estuary is net heterotrophic and that the majority of heterotrophy (NEP < 0) in the estuary occurs in Plum Island Sound (15–24 km) (Table 1). Furthermore, the presence of several local minima do not significantly degrade the estimation of NEP, as evident by the small NEP standard deviations (Table 1).

8. Discussion

Our oxygen metabolism model, Eqs. (1)–(4), accounts for advective and dispersive transport processes, oxygen exchange with the atmosphere, oxygen input from lateral sources, and oxygen production and consumption by biological processes. To determine the relative importance of each of these processes at a particular location and time, it is necessary to analyze each term in Eq. (1) separately. By far the dominant terms in the oxygen balance are gross primary production, $P(\bar{x},t)$, and community respiration, $R(\bar{x})$. To examine the contribution of the other terms, a cubic spline was fit to the simulated oxygen concentration, $\hat{c}_{\mathrm{O_2}}(\bar{x},t_n)$, then the following respiration-normalized terms were calculated at time $t_{\mathrm{E}} = 1.25$ d,

Table 1
Cumulative, daily averaged gross production, community respiration and net ecosystem productivity (Eq. (17)) over whole estuary and subsections for best optimal solution

Section (km)	$\langle P(\bar{x}_{\mathrm{U}}\|\bar{x}_{\mathrm{D}})\rangle_{\Sigma}$	$\langle R(\bar{x}_{\mathrm{U}}\|\bar{x}_{\mathrm{D}})\rangle_{\Sigma}$	$\langle N(\bar{x}_{\mathrm{U}}\|\bar{x}_{\mathrm{D}})\rangle_{\Sigma}$
0–5	0.87 (0.04)	0.94 (0.04)	−0.076 (0.006)
5–10	1.7 (0.1)	2.2 (0.1)	−0.48 (0.02)
10–15	6.1 (0.7)	6.8 (0.7)	−0.77 (0.04)
15–24	39 (7)	43 (7)	−3.5 (0.5)
Whole estuary	48 (7)	53 (7)	−4.8 (0.5)

Rates are in Mg C d^{-1} with standard deviation from all 10 local optima solutions in parentheses.

dispersion :

$$\frac{\partial}{\partial \bar{x}}\left(D(\bar{x})A(\bar{x})\frac{\partial \hat{c}_{O_2}(\bar{x}, t_E)}{\partial \bar{x}}\right)/(A(\bar{x})R(\bar{x})) \tag{18}$$

advection :

$$-\frac{\partial}{\partial \bar{x}}(q(\bar{x}, t_E)\hat{c}_{O_2}(\bar{x}, t_E))/(A(\bar{x})R(\bar{x})) \tag{19}$$

lateral inputs :

$$\sum_{i=1}^{6}\left(c_{li}(t)\frac{\partial q_i(\bar{x}, t_E)}{\partial \bar{x}}\right)/(A(\bar{x})R(\bar{x})) \tag{20}$$

gas invasion :

$$\frac{k_{O_2}}{h(\bar{x})}(c^*_{O_2}(c_S, T) - \hat{c}_{O_2}(\bar{x}, t_E))/R(\bar{x}) \tag{21}$$

The analysis shows that the two dominant terms are gas invasion and dispersion, accounting for approximately 21 and 14% of oxygen accumulation or loss relative to $R(\bar{x})$, respectively (Fig. 11). Not accounting for these terms would introduce significant errors in estimating $P(\bar{x}, t)$ and $R(\bar{x})$. Both advection and lateral inputs are small, but these terms would be larger during higher freshwater discharge periods. Indeed, analysis of the *Pe* number (Fig. 2) indicates these terms should dominate under high discharge in the upper reaches of the estuary.

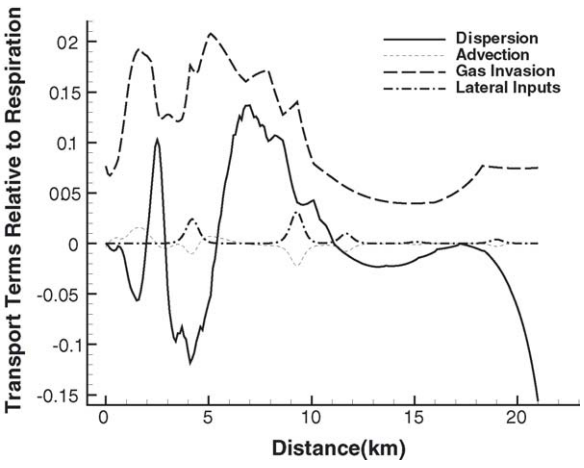

Fig. 11. Contribution of dispersion, advection, gas invasion and lateral inputs to oxygen accumulation rate as a function of location along estuarine axis relative to community respiration evaluated at 6:00 28 June 1995 for $J = 12{,}400$ solution.

Analysis of Eqs. (18)–(21) indicates which terms are important in Eq. (1) at a particular instant, but they are not in proper form to assess the fate of oxygen in the estuary. To understand the latter, we can look at the net accumulation and input of oxygen in the estuary integrated over the time transect data were collected, as given by,

$$\begin{aligned}
&\frac{1}{\Delta t}\int_{\bar{x}_U}^{\bar{x}_D}\hat{c}_{O_2}(\bar{x}, \tau)A(\bar{x})\,d\bar{x}\Big|_{\tau=t}^{\tau=t+\Delta t} \\
&= \frac{1}{\Delta t}\int_t^{t+\Delta t}\int_{\bar{x}_U}^{\bar{x}_D}(P(\bar{x}, t) - R(\bar{x}))A(\bar{x})\,d\bar{x}\,dt \\
&\quad + \frac{1}{\Delta t}\int_t^{t+\Delta t}\int_{\bar{x}_U}^{\bar{x}_L}k_{O_2}(c^*_{O_2}(\bar{x}, T) \\
&\quad - \hat{c}_{O_2}(\bar{x}, t))\frac{A(\bar{x})}{h(\bar{x})}\,d\bar{x}\,dt \\
&\quad + \frac{1}{\Delta t}\int_t^{t+\Delta t}\left(q(\bar{x}, t)c_{O_2}(\bar{x}, t) - D(\bar{x})A(\bar{x})\right. \\
&\quad \left.\times\frac{\partial c_{O_2}(\bar{x}, t)}{\partial \bar{x}}\right)dt\Big|_{\bar{x}=\bar{x}_D}^{\bar{x}=\bar{x}_U} \\
&\quad + \frac{1}{\Delta t}\int_{\bar{x}_U}^{\bar{x}_D}\sum_{i=1}^{\ell}\left(c_{O_2 i}(t)\frac{\partial q_i(\bar{x}, t)}{\partial \bar{x}}\right)d\bar{x}
\end{aligned} \tag{22}$$

The left-hand side of Eq. (22) is the oxygen accumulation in the estuary over time Δt and the four terms on the right-hand side are oxygen imports over Δt due to net ecosystem production, exchange with the atmosphere, water transport across the boundaries, and lateral inputs, respectively. Solution of Eq. (22) over the whole estuary for the 2 days transect data were collected gives an oxygen net accumulation (in kmol O_2 d^{-1}) of -404, which balances an NEP of -398, plus a net O_2 invasion of 34.3, plus -56.2 net longitudinal import, plus 15.9 from lateral inputs. Since O_2 inputs ($34.2 + 15.9$ kmol d^{-1}) approximately balance net transport (-56.2 kmol d^{-1}), the NEP of -398 kmol d^{-1} leads to a net decrease in estuarine oxygen concentration, which indicates the estuary is not at steady state. For the York River, Raymond et al. (2000) found that gas evasion could account for between 50 and 100% of NEP; however, they assume the river was at steady state, which is not the situation for PIE when sampled. In a Chesapeake Bay study, Kemp

and Boynton (1980) found gas exchange to be a small component of the oxygen budget (∼5%) and horizontal transport accounted for approximately 40–50% of the change on O_2. However, their analysis was not tidally averaged (as is this study), which could account for the large horizontal transport terms. If we look at net O_2 changes at their stations CC_7 and KB_4, we find that O_2 estuarine accumulation often dominates the O_2 budget and is balanced largely by horizontal transport, which also indicates that the system was not at steady state during their study. In the Ems-Dollard Estuary, an annually averaged oxygen balance shows that the large negative NEP observed is balanced almost entirely by gas exchange across the air–water interface (Van Es and Ruardij, 1982). Perhaps not surprisingly, our work in combination with these others shows that the dominant terms of the oxygen balance equation are system dependent and that the estuary may or may not be at steady state conditions when sampled.

The sag in dissolved oxygen concentration between 14 and 28 PSU (Fig. 3) with a minimum at 22 PSU is due mostly to a decrease in NEP (Fig. 7) that is caused by a large decrease in GPP, with only a small decrease in CR. Water column depth does not appear to be a significant factor, because water depth increases continuously from 1.4 m at 0 PSU to 5.7 m at 28 PSU, then decreases to 3.7 m at 31 PSU. If depth were a significant contributor to the DO sag, then we would expect the DO minimum to occur at 28 and not 22 PSU.

Except at a few limited locations, PIE is net heterotrophic over the period of study (Table 1, Fig. 10), which is consistent with the general finding regarding metabolic status of most marsh-dominated estuaries (Howarth et al., 1996; Smith and Hollibaugh, 1997; Cai et al., 1999; Raymond et al., 2000). The depth integrated rates of metabolism (Fig. 9) are also well within those found for other similar estuaries (Wilson, 2002), indicating that PIE is typical. However, our transect-based inverse modeling approach does provide for greater spatial resolution than standard methods and does reveal locations where net autotrophy occurs. Standard approaches to estimating NEP would likely miss these features, which can shift in location due to the variability in freshwater discharge and the transport characteristics of PIE (Fig. 2). For example, estuarine fisheries are subject to freshet events that can displace or wash out phytoplankton blooms, which planktivores depend on for food (Drinkwater, 1986). By locating and tracking areas of high primary productivity, it may be possible to better assess impacts of freshwater discharge on secondary consumers.

Although the fit between observed and predicted DO concentration is good (Fig. 4), it is likely a better fit could be obtained by accounting for the following approximations. Our current model for $P(\bar{x}, t)$, Eq. (8), does not account for light saturation, which has been observed to occur (Portielje et al., 1996), and may explain the weaker model fits at 11:00 (Fig. 4(C)) and 7:15 (Fig. 4(F)). We choose not to include light saturation because it would introduce another parameter. We also used a fixed value for the gas exchange parameter, k_{O_2}, that was estimated by other methods. It is possible to treat k_{O_2} as an unknown, or an unknown function of location, $k_{O_2}(\bar{x})$, and to include this parameter, or parameters, in the minimization search, Eq. (10). Analysis of Eq. (1) shows that $k_{O_2}(\bar{x})$ is observable from DO measurements only; however, estimation of $k_{O_2}(\bar{x})$ was not investigated in this study.

Negative NEP in PIE (Table 1) means a significant amount of carbon is being respired within the estuary. There are three possible sources for this allochthonous carbon: (1) terrestrial organic carbon (OC) in freshwater inputs, (2) OC from the marsh platform, or (3) marine OC. The average freshwater discharge at the Byfield USGS gaging station during the period when transects were conducted was $0.058\,m^3\,s^{-1}$ (or $5040\,m^3\,d^{-1}$). Using watershed-size weighting factors on the Byfield discharge (Vallino and Hopkinson, 1998), gives a total freshwater input to PIE of $0.64\,m^3\,s^{-1}$ (or $55600\,m^3\,d^{-1}$). During the summer period in the Parker and Ipswich Rivers, particulate organic carbon (POC) and dissolved organic carbon (DOC) average 74 and 850 μM, respectively (Peterson et al., 1995; Raymond and Bauer, 2001) (also see http://ecosystems.mbl.edu/PIE). Based on these values, total freshwater carbon loading was $0.62\,Mg\,C\,d^{-1}$, of which perhaps 15% could be degraded in the estuary based on bioassay studies and water residence time (Uhlenhopp et al., 1995). Likely respiration of the instantaneous terrestrial OC inputs would amount to only $0.092\,Mg\,C\,d^{-1}$, or only 2% of the observed NEP (Table 1). Consequently, terrestrial OC inputs cannot account for the magnitude of NEP in PIE.

Above ground marsh productivity at PIE has been measured at $294\,g\,C\,m^{-2}\,y^{-1}$ (Ruber et al., 1981),

which falls within the range 200–600 g C y^{-1} measured at other sites if we assume 50% dry weight is carbon (Blum et al., 1978; Reidenbaugh, 1983; Morris and Haskin, 1990). Given that growth occurs over a 4-month period at PIE, this gives a potential marsh export of 2.4 g C m^{-2} d^{-1}. This would amount to a total production of 95.5 Mg C d^{-1} from the 39.8 km^2 of PIE marsh. Even if only 5% of this carbon were respired in the estuarine water column, it would be more than enough to support the observed NEP over the whole estuary (Table 1). Hence, marsh exports, or respiration directly on the marsh platform (Cai et al., 1999, 2000), appear to be a likely candidate for explaining the NEP observed in PIE. Stable- and radioisotope surveys in PIE also support significant marsh exports (Raymond and Hopkinson, 2003).

As for the marine OC, this is more difficult to estimate, but we can use the age of marine OC in the estuary combined with its expected decomposition rate to estimate the marine OC contribution to total respiration. The average age of saltwater in PIE at the observed freshwater discharge is approximately 3 days (Vallino and Hopkinson, 1998). The volume of saltwater in the estuary is given by

$$V_{SW} = \frac{1}{c_{S_O}} \int_0^{24{,}000} c_S(\bar{x}) A(\bar{x})\, d\bar{x} \tag{23}$$

where c_{S_O} is the salinity of the marine end member, which was 31 PSU. From the predicted high tide salinity distribution from Eq. (1), V_{SM} equals 38.8×10^6 m^3 during the study period. Bioassay studies on the degradability of marine OC on the continental margin indicates DOC decomposition can be accurately assessed using a three pool model, consisting of very labile, labile, and refractory components (Hopkinson et al., 2002). Using this model and assuming a marine OC concentration of 100 μM consisting of 16% very labile, 13% labile and 71% refractory with decomposition rate coefficients of 0.219 d^{-1} (k_1) and 0.018 d^{-1} (k_2) for the very labile and labile pools, respectively (Hopkinson et al., 2002), we estimate that 8.4 μM of marine DOC would be respired over a 3-day period (or 2.8 μM d^{-1}). This decomposition rate combined with the saltwater volume, V_{SW}, gives a C respiration of 1.3 Mg C d^{-1} in the estuary originating from the marine end member. This estimate indicates that approximately 27% of the observed estuarine respiration (Table 1) originates from the marine end member. Since only 2% of estuarine respiration can be attributed to terrestrial inputs, 71% of the respiration must come from marsh inputs to the water column.

This analysis is only applicable for the days studied, 27–29 June 1995. More transects studies must be conducted throughout the year before we can be definitive in regards to the auto- or heterotrophic state of the estuary, and whether or not this state changes over the year. It is also likely the dominant sources of respired carbon will change over the year, especially during high spring discharge when terrestrial inputs are much larger.

9. Conclusions

Our advection–dispersion model combined with near-synoptic DO sampling method and nonlinear inverse technique is able to produce detailed spatial estimates for gross primary production, community respiration and net ecosystem production in Plum Island Estuary. The approach is generally applicable to any vertically well-mixed estuary, and can be extended to stratified estuaries provided spatially appropriate transport models are available. Analysis of the transport equation at any given time slice reveals that air-water gas exchange and longitudinal dispersion can account for up to 21 and 14% of local DO accumulation relative to respiration, respectively. However, analysis averaged over a 2-day time period shows that the negative estuarine NEP is balanced almost entirely by a decrease in estuarine oxygen storage. The results obtained from DO transects conducted in June 1995 indicate that PIE is a net heterotrophic system (-4.8 Mg C d^{-1}) with the majority of allochthonous C inputs originating from the extensive tidal marshes (71%), followed by marine organic carbon (27%) and terrestrial inputs (2%).

Acknowledgements

We thank Ishi Buffam, Brian Balsis and David Alderman for their assistance during the field component of this research. This research was supported by NSF grant OCE-9726921.

References

Baker, K.S., Frouin, R., 1987. Relation between photosynthetically available radiation and total insolation at the ocean surface under clear skies. Limnol. Oceanogr. 32, 1370–1377.

Blom, J.G., Zegeling, P.A., 1994. Algorithm 731: a moving-grid interface for systems of one-dimensional time-dependent partial differential equations. ACM Trans. Math. Software 20, 194–214.

Blum, U., Seneca, E.D., Stroud, L.M., 1978. Photosynthesis and respiration of Spartina and Juncus salt marshes in North Carolina: some models. Estuaries 1, 228–238.

Blumberg, A., Signell, R., Jenter, H., 1993. Modeling transport processes in the coastal ocean. J. Mar. Environ. Eng. 1, 31–52.

Box, M.J., 1966. A comparison of several current optimization methods, and the use of transformations in constrained problems. Comput. J. 9, 67–77.

Brent, R.P., 1973. Algorithms for Minimization Without Derivatives. Prentice-Hall, New Jersey, pp. 195.

Brock, T.D., 1981. Calculating solar radiation for ecological studies. Ecol. Model. 14, 1–19.

Caffrey, J.M., Cloern, J.E., Grenz, C., 1998. Changes in production and respiration during a spring phytoplankton bloom in San Francisco Bay, California, USA: implications for net ecosystem metabolism. Mar. Ecol. Prog. Ser. 172, 1–12.

Cai, W.-J., Pomeroy, L.R., Moran, M.A., Wang, Y., 1999. Oxygen and carbon dioxide mass balance for the estuarine-intertidal marsh complex of five river in the southeastern U.S. Limnol. Oceanogr. 44, 639–649.

Cai, W.-J., Wiebe, W.J., Wang, Y., Sheldon, J.E., 2000. Intertidal marsh as a source of dissolved inorganic carbon and a sink of nitrate in the Satilla River–estuarine complex in the southeastern U.S. Limnol. Oceanogr. 45, 1743–1752.

Carini, S., Weston, N., Hopkinson, C., Tucker, J., Giblin, A.E., Vallino, J., 1996. Gas exchange in the Parker River estuary, Massachusetts. Biol. Bull. 191, 333–334.

Cole, J.J., Pace, M.L., Carpenter, S.R., Kitchell, J.F., 2000. Persistence of net heterotrophy in lakes during nutrient addition and food web manipulations. Limnol. Oceanogr. 45, 1718–1730.

Dongarra, J.J., Grosse, E., 1987. Distribution of mathematical software via electronic mail. Commun. Assoc. Comput. Mach. 30, 403–407.

Drinkwater, K.F., 1986. On the role of freshwater outflow on coastal marine ecosystems: A workshop summary. In: Skreslet, S. (Ed.), The Role of Freshwater Outflow in Coastal Marine Ecosystems. Springer-Verlag, Berlin, pp. 429–438.

Fenneman, N.M., 1938. Physiography of the Eastern United States. McGraw-Hill, New York, 714.

Gaarder, T., Gran, H.H., 1927. Investigations of the production of plankton in the Olso Fjord. Rapports et Procés-Verbaux Des Réunions. Conseil Permanent International Pour L'exploration De La Mer 42, 1–48.

Genereux, D.P., Hemond, H.F., 1992. Determination of gas exchange rate constants for a small stream on walker branch watershed, Tennessee. Water Resour. Res. 28, 2365–2374.

Geyer, W.R., Signell, R.P., 1992. A reassessment of the role of tidal dispersion in estuaries and bays. Estuaries 15, 97–108.

Gulliver, J.S., Stefan, H.G., 1984a. Stream productivity analysis with DORM: I development of computation model. Water Res. 18, 1569–1576.

Gulliver, J.S., Stefan, H.G., 1984b. Stream productivity analysis with DORM: II parameter estimation and sensitivity. Water Res. 18, 1577–1588.

Gulliver, J.S., Stefan, H.G., 1984c. Stream productivity analysis with DORM: III productivity of experimental streams. Water Res. 18, 1589–1595.

Hansen, D.V., Rattray, M., 1966. New dimensions in estuary classification. Limnol. Oceanogr. 11, 319–325.

Hopkinson, C.S., 1985. Shallow-water benthic and pelagic metabolism: evidence of heterotrophy in the nearshore Georgia Bight. Mar. Biol. 87, 19–32.

Hopkinson, J., Vallino, J.J., Nolin, A., 2002. Decomposition of dissolved organic matter from the continental margin. Deep Sea Res. Part II: Topical Stud. Oceanogr. 49, 4461–4478.

Hornberger, G.M., Kelly, M.G., 1972. The determination of primary production in a stream using an exact solution to the oxygen balance equation. Water Res. Bull. 8, 795–801.

Howarth, R.W., Schneider, R., Swaney, D., 1996. Metabolism and organic carbon fluxes in the tidal freshwater Hudson River. Estuaries 19, 848–865.

Jahne, B., Munnich, K.O., Bosinger, R., Dutzi, A., Huber, W., Libner, P., 1987. On the parameters influencing air-water gas exchange. J. Geophys. Res. 92, 1937–1949.

Kelly, M.G., Hornberger, G.M., Cosby, B.J., 1974. Continuous automated measurement of rates of photosynthesis and respiration in an undisturbed river community. Limnol. Oceanogr. 19, 305–312.

Kemp, W.M., Boynton, W.R., 1980. Influence of biological and physical processes on dissolved oxygen dynamics in an estuarine system: implications for measurement of community metabolism. Estuarine Coastal Mar. Sci. 11, 407–431.

Kemp, W.M., Smith, E.M., Marvin-DiPasquale, M., Boynton, W.R., 1997. Organic carbon balance and net ecosystem metabolism in Chesapeake Bay. Mar. Ecol. Prog. Ser. 150, 229–248.

Laws, E.A., 1991. Photosynthetic quotients, new production and net community production in the open ocean. Deep-Sea Res. 38, 143–167.

Leclercq, N., Gattuso, J., Jaubert, J., 1999. Measurement of oxygen metabolism in open-top aquatic mesocosms: application to a coral reef community. Mar. Ecol. Prog. Ser. 177, 299–304.

Madden, C.J., Day Jr., J.W., 1992. An instrument system for high-speed mapping of chlorophyll a and physico-chemical variables in surface waters. Estuaries 15, 421–427.

Marzolf, E.R., Mulholland, P.J., Steinman, A.D., 1994. Improvements to the diurnal upstream–downstream dissolved oxygen change technique for determining whole-stream metabolism in small streams. Can. J. Fish. Aquat. Sci. 51, 1591–1599.

Morris, J.T., Haskin, B., 1990. A 5-yr record of aerial primary production and stand characteristics of *Spartina alterniflora*. Ecology 71, 2209–2217.

Mulholland, P.J., Ellows, C.S., Tank, J.L., Grimm, N.B., Webster, J.R., Hamilton, S.K., Marti, E., Ashkenas, L., Bowden, W.B., Dobbs, W.K., McDowell, W.H., Paul, M.J., Peterson,

B.J., 2001. Inter-biome comparison of factors controlling stream metabolism. Freshwater Biol. 46, 1503–1517.

Odum, H.T., 1956. Primary production in flowing waters. Limnol. Oceanogr. 1, 102–117.

Odum, H.T., Hoskin, C.M., 1958. Comparative studies in the metabolism of marine waters. Publications of the Institute of Marine Sciences. Contributions 5, 16–46.

Park, K., Kuo, A.Y., Neilson, B.J., 1996. A numerical model study of hypoxia in the tidal Rappahannock River of Chesapeake Bay. Estuarine Coastal Shelf Sci 42, 563–581.

Parkhill, K.L., Gulliver, J.S., 1999. Modeling the effect of light on whole-stream respiration. Ecol. Modell. 117, 333–342.

Perez, F.F., Alvarez-Salgado, X.A., Roson, G., 2000. Stoichiometry of the net ecosystem metabolism in a coastal inlet affected by upwelling. The Ria de Arousa (NW Spain). Mar. Chem. 69, 217–236.

Peterson, B., Fry, B., Hullar, M., Saupe, S., Wright, R., 1995. The distribution and stable carbon isotopic composition of dissolved organic carbon in estuaries. Estuaries 17, 111–121.

Portielje, R., Kersting, K., Lijklema, L., 1996. Primary production estimation from continuous oxygen measurements in relation to external nutrient input. Water Res. 30, 625–643.

Raymond, P.A., Bauer, J.E., 2001. Riverine export of aged terrestrial organic matter to the North Atlantic Ocean. Nature 409, 497–500.

Raymond, P.A., Bauer, J.E., Cole, J.J., 2000. Atmospheric CO2 evasion, dissolved inorganic carbon production, and net heterotrophy in the York River estuary. Limnol. Oceanogr. 45, 1707–1717.

Raymond, P.A., Hopkinson, C.S., 2003. Ecosystem modulation of dissolved carbon age in a temperate marsh-dominated estuary. Ecosystems 6, 694–705.

Reidenbaugh, T.G., 1983. Productivity of cordgrass, *Spartina alterniflora*, estimated from live standing crops, mortality, and leaf shedding in a Virginia salt marsh. Estuaries 6, 57–65.

Renka, R.J., 1996a. Algorithm 752; SRFPACK: software for scattered data fitting with a constrained surface under tension. ACM Trans. Math. Software 22, 9–17.

Renka, R.J., 1996b. Algorithm 751; TRIPACK: a constrained two-dimensional Delaunay triangulation package. ACM Trans. Math. Software 22, 1–8.

Robinson, C., Williams, P.J., 1999. Plankton net community production and dark respiration in the Arabian Sea during September 1994. Deep Sea Res. Part II: Topical Stud. Oceanogr. 46, 745–765.

Ruber, E., Gillis, G., Montagna, P.A., 1981. Production of dominant emergent vegetation and of pool algae on a norther Massachuessetts salt marsh. Bull. Torrey Bot. Garden 180, 180–188.

Sammel, E.A., 1967. Water resources of the Parker and Rowley River basins Massachusetts. U.S. Geological Survey, Hydrologic Investigations HA-247, 9 pp.

Smith, R., 1977. Long-term dispersion of contaminants in small estuaries. J. Fluid Mech. 82, 129–146.

Smith, S.V., Hollibaugh, J.T., 1997. Annual cycle and interannual variability of ecosystem metabolism in a temperate climate embayment. Ecol. Monogr. 67, 509–533.

Swaney, D., Howarth, R.W., Butler, T.J., 1999. A novel approach for estimating ecosystem production and respiration in estuaries: application to the oligohaline and mesohaline Hudson River. Limnol. Oceanogr. 44, 1509–1521.

Uhlenhopp, A.G., Hobbie, J.E., Vallino, J.J., 1995. Effects of land use on the degradability of dissolved organic matter in three watersheds of the Plum Island Sound Estuary. Biol. Bull. 189, 256–257.

Vallino, J.J., 2000. Improving marine ecosystem models: use of data assimilation and mesocosm experiments. J. Mar. Res. 58, 117–164.

Vallino, J.J., Hopkinson, C.S., 1998. Estimation of dispersion and characteristic mixing times in Plum Island Sound estuary. Estuarine Coast. Shelf Sci. 46, 333–350.

Van Es, F.B., Ruardij, P., 1982. The use of a model to assess factors affecting the oxygen balance in the water of the Dollard. Neth. J. Sea Res. 15, 313–330.

Vandevender, W.H., Haskell, K.H., 1982. The SLATEC mathematical subroutine library. SIGNUM Newslett. 17, 16–21.

Weiss, R., 1970. The solubility of nitrogen, oxygen and argon in water and seawater. Deep Sea Res. 17, 721–735.

Welch, H.E., 1968. Use of modified diurnal curves for the measurement of metabolism in standing water. Limnol. Oceanogr. 13, 679–687.

Williams, P.J.L.B., Robertson, J.E., 1991. Overall plankton oxygen and carbon dioxide metabolisms: The problem of reconciling observations and calculations of photosynthetic quotients. J. Plankton Res. 13, 153–169.

Wilson, J.G., 2002. Productivity, Fisheries and Aquaculture in Temperate Estuaries. Estuarine Coastal Shelf Sci. 55, 953–967.

Young, R.G., Huryn, A.D., 1998. Comment: Improvements to the diurnal upstream-downstream dissolved oxygen change technique for determining whole-stream metabolism in small streams. Can. J. Fish. Aquat. Sci. 55, 1784–1785.

Young, R.G., Huryn, A.D., 1999. Effects of land use on stream metabolism and organic matter turnover. Ecol. Appl. 9, 1359–1376.